

High performance integrated solar combined cycles with minimum modifications to the combined cycle power plant design



Giovanni Manente

Department of Industrial Engineering, University of Padova, Via Venezia 1, 35131 Padova, Italy

ARTICLE INFO

Article history:

Received 12 October 2015

Accepted 20 December 2015

Available online 7 January 2016

Keywords:

Natural gas combined cycle
Integrated solar combined cycle
Off-design behavior
Solar energy
Solar share
Retrofitting

ABSTRACT

The integration of solar energy into natural gas combined cycles has been successfully demonstrated in several integrated solar combined cycles since the beginning of this decade in many countries. There are many motivations that drive investments on integrated solar combined cycles which are primarily the repowering of existing power plants, the compliance with more severe environmental laws on emissions and the mitigation of risks associated with large solar projects. Integrated solar combined cycles are usually developed as brownfield facilities by retrofitting existing natural gas combined cycles and keeping the existing equipment to minimize costs. In this work a detailed off-design model of a 390 MW_e three pressure level natural gas combined cycle is built to evaluate different integration schemes of solar energy which either keep the equipment of the combined cycle unchanged or include new equipment (steam turbine, heat recovery steam generator). Both power boosting and fuel saving operation strategies are analyzed in the search for the highest annual efficiency and solar share. Results show that the maximum incremental power output from solar at design solar irradiance is limited to 19 MW_e without modifications to the existing equipment. Higher values are attainable only including a larger steam turbine. High solar radiation-to-electrical efficiencies in the range 24–29% can be achieved in the integrated solar combined cycle depending on solar share and extension of tube banks in the heat recovery steam generator. Compared to power boosting, the fuel saving strategy shows lower thermal efficiencies of the integrated solar combined cycle due to the efficiency drop of gas turbine at reduced loads. Without modifications to the existing equipment the maximum solar share of the total generated electricity is only about 1%.

© 2016 Elsevier Ltd. All rights reserved.

1. Introduction

Several integrated solar combined cycles (ISCCs) are in operation all around the world (North Africa, Iran, Italy, USA) and many projects are underway (Mexico, China, USA), as reviewed in [1]. ISCCs offer many advantages compared to solar thermal power plants, primarily associated with the higher solar energy conversion efficiency and the lower investment costs [2]. Investors and owners are attracted by the mitigated risk associated with the construction of smaller solar fields compared to solar thermal power plants [3].

Many papers have appeared since the late nineties [4] about the thermodynamic analysis of ISCCs focusing on the optimum integration point of solar energy into the combined cycle. Kelly et al. [5] demonstrated that the most efficient way for converting solar thermal energy into electricity is to withdraw feed water from the heat recovery steam generator (HRSG) downstream of the last

economizer, to produce high pressure saturated steam and to return the steam to the HRSG for superheating and reheating. Rovira et al. [6] end up with the same conclusion finding that the highest incremental solar thermal-to-electrical efficiency (44.6%) is achieved when solar heat is used for the evaporation process and eventually for superheating, but not for preheating feed water. Li and Yang [7] proposed a novel ISCC where both high and low pressure saturated steam are generated from solar to increase the solar share. This system was found to reach high solar radiation-to-electric efficiency (up to 30%) due to the improvement of the thermal match in the HRSG. Montes et al. [8] considered a 50 MW_{th} hybridization size in a 220 MW_e natural gas combined cycle (NGCC) with the preheating and boiling processes directly accomplished in the parabolic trough collectors. The incremental electricity from solar compensated the gas turbine power drop at high ambient temperatures. Baghernejad and Yaghoubi [9] quantified the exergy destruction in all plant subsystems and found that the least efficient component is the solar collector. Libby et al. [10] showed that the highest thermodynamic performance is obtained

E-mail address: giovanni.manente@unipd.it

Nomenclature

A	heat transfer area, m ²
ANI	aperture normal irradiance, W/m ²
LMTD	log-mean temperature difference, K
\dot{m}	mass flow rate, kg/s
p	pressure, bar
q	heat load, kW
T	temperature, °C, K
U	overall heat transfer coefficient, W/(m ² K)
\dot{W}	power output, kW

Greek symbols

φ	flow function
η	efficiency
ρ	density, kg/m ³
ΔT_{min}	minimum temperature difference, °C
ΔW	power output difference, kW

Subscripts

amb	ambient
$coll$	solar collector
$corr$	corrected
DP	design point
EXG	exhaust gases
in	inlet
$incr$	incremental
out	outlet

sol	solar
ST	steam
th	thermal

Acronyms and abbreviations

CCT	minimum load to keep steam superheating and reheating temperatures at nominal values
CMA	minimum load to keep gas turbine emissions below environmental limits
CMT	minimum load to preserve the equipment
CNC	continuous nominal load
CSP	concentrating solar power
GT	gas turbine
HP	high pressure
HPT	high pressure turbine
HRSG	heat recovery steam generator
IP	intermediate pressure
IPT	intermediate pressure turbine
LCOE	levelized cost of electricity
LP	low pressure
LPT	low pressure turbine
PR	pressure ratio
ST	steam turbine
VGW	variable guide vanes

with solar steam generated at the highest temperature and pressure and fed upstream the high pressure turbine. Peterseim et al. [11] compared different concentrating solar power (CSP) technologies (parabolic trough, linear Fresnel and solar tower) for integration of 80 MW_{th} from CSP into a 200 MW_e NGCC on the basis of various criteria related to feasibility, risk, environmental impact and levelized cost of electricity (LCOE). They found that Fresnel solar collectors ranked best followed by parabolic troughs using thermal oil as heat transfer fluid.

The higher conversion efficiency of solar energy in ISCCs in combination with the equipment shared with the NGCC results in a lower solar LCOE compared to solar thermal power plants which could be the driving force for a massive deployment of this technology. For instance, in [12] the solar LCOE were calculated equal to 9.8 and 11.3 c\$/kW h for an ISCC and a solar thermal power plant, respectively, both located in Barstow (CA, USA). In [13] the cost of electricity of the overall ISCC power plant was estimated in the range between 4.5 and 5.7 c€/kW h depending on the extension of the solar field. A higher value of approximately 7.5 c\$/kW h was calculated for the overall plant in [14] due to the higher solar share. Antonanzas et al. [15] evaluated the potential of solar thermal integration into thirty NGCCs in Spain without modifications to the existing design. A similar analysis carried out in [16] for three NGCCs in Algeria showed that the increase in yield was up to 9.2 GW h/year for each power plant and the solar incremental LCOE was only 9.5 c\$/kW h. On the other hand, Trad and Ali [17] calculated a much higher LCOE approaching 25 c€/kW h for a 100 MW_e solar thermal power plant located in Algeria. This marked spread between solar thermal plants and ISCCs clearly asks for a new pricing regulation promoting the deployment of the latter and, in general, of hybrid solar-fossil fuel power plants with a relatively low solar share. In countries with high coal consumption like China the interest is on the hybridization of coal-fired power

plants [18] in so-called “solar aided coal-fired power generation systems” (SACPGS), which enables high solar-to-electricity conversion efficiencies as well. Peng et al. [19] analyzed the hybridization of a 330 MW_e coal-fired power plant where a solar-driven feed water heater is added in parallel with the last preheater to reduce the extraction from the steam turbine. They found that the solar radiation-to-electrical efficiency can reach 27.3% (1.4%-points higher than the solar thermal power plant) and that the LCOE can be reduced to 12.6–15.8 c\$/kW h, about 20–30% lower than solar thermal power plants.

The main limitation in both ISCCs and SACPGS is the low solar share achievable. A concept to increase the solar share is to co-locate CSP facilities with simple-cycle gas turbines which transfer the exhaust heat to the heat transfer fluid of the solar plant [20]. Guédez et al. [21] evaluated the performance of such a plant including a 100 MW_e gas turbine and a 60 MW_e molten-salt solar tower with storage and calculated LCOE values for the total plant in the range 11.0–12.2 c\$/MW h. A higher solar share up to 90% [22] is achievable when solar energy is integrated in the topping part of a NGCC to preheat compressed air ahead of the combustion chamber, an integration scheme that has already demonstrated technical feasibility in the Solugas project [23].

The development of several ISCCs projects, in a country like Italy, having a high natural gas consumption and a high availability of solar energy can represent an important step for a gradual abatement of CO₂ emissions in the generation sector, and for the promotion of cost-effective CSP technologies. The optimization of the annual performance and the selection of a proper design point are critical for the economics of such systems. Combined cycles with solar integration often operate at off-design conditions due to the intrinsic variable nature of solar energy and because of retrofit schemes searching for minimum modifications to the existing equipment (steam turbines, HRSG). Thus, to check both feasibility

and performance of different integration options it is essential to take part load behavior of the main plant components into account. Some papers recently appeared in the literature accurately describe the design and off-design behavior of ISCCs using commercial software (IPSEpro[®], Thermoflex[®], GateCycle[®], Epsilon[®]). Zhu et al. [24] developed a model of a three pressure level NGCC with solar integration using the software IPSEpro[®]. When solar heat is integrated into the system the duct burner is turned off to reserve enough capacity room in the steam turbine. They calculated solar thermal-to-electrical efficiencies in the range between 40% and 45% (depending on solar thermal input) which are significantly higher (approximately 10%-points higher) than the steam cycle efficiency. The overall power boost from solar reached 83 MW_e (from 475 MW_e to 558 MW_e) which corresponds to a solar share of about 17%. Gülen [25] evaluated external heat addition from solar at high, intermediate and low pressure HRSG sections in the Thermoflex[®] environment, and found that the highest incremental solar thermal-to-electrical efficiency ($\approx 46\%$) is obtained with HP steam generation and feed water take-off directly upstream the evaporator at moderate solar fractions (<8%). Ojo et al. [26] based the integration study on a modern Alstom combined cycle power plant by using a proprietary performance calculation tool. The authors chose the outlet of condensate pump as feed point to the solar field and the inlet of HP steam turbine (560 °C) as solar injection point, and found that up to 15% power boost (about 70 MW_{el}) can be obtained by operating the GT at full load provided that the swallowing capacity of the HP is increased. Alternatively, solar steam can be integrated in operating combined cycles keeping the existing steam turbine and HRSG unchanged. In such conditions the maximum drum pressure in the HP circuit is reached at 55 MW_{th} solar thermal load which allows boosting the power output of the combined cycle up to about 4.5%. They calculated a solar thermal-to-electrical conversion efficiency equal to 35%. Pihl et al. [27] developed a thermo-economic optimization model of a 400 MW_e triple pressure combined cycle retrofitted with solar trough collectors using the Epsilon[®] modeling software. Two conflicting objective functions were considered in a multi-objective optimization: the minimization of the total required investment and the maximization of the net present value. The sizing of the solar field, the gas turbine load and the extra steam turbine capacity were selected as decision variables. Results showed that the optimal integration of the ISCC asks for a high gas turbine load (>80%) and a larger steam turbine. Solar integration was found to be limited to a 4% solar share (i.e., 16 MW_e). The LCOE was found to be 10 c€/kWh which is much lower than the typical LCOE of a conventional solar thermal power plant (17–19 c€/kWh).

All mentioned studies have emphasized the need of a systematic analysis, still missing in the literature, to identify the integration limits of solar energy into existing combined cycles and to choose the best strategies (new equipment and/or modifications to the plant's operation) to maximize the performance. This work addresses these topics through a systematic comparison of different hybridization options. A detailed off-design model of an operating three pressure levels NGCC is built in the Thermoflex[®] environment to form the basis of an accurate ISCC study. Two different integration strategies of solar energy into the reference NGCC are considered: power boosting and fuel saving. The former aims at increasing the NGCC power output, the latter at reducing natural gas consumption while keeping power output constant. Multiple retrofitting options are considered for both strategies which keep different parts (steam turbine, HRSG) of the original NGCC in the ISCC system unaltered. The performance deriving from different strategies and scenarios are compared in the search for the highest annual plant efficiency and solar share.

2. Off-design behavior of the natural gas combined cycle power plant

In this section the off-design behavior of the three pressure level NGCC plant located in Priolo Gargallo (Sicily, Italy) is analyzed by means of a simulation model developed in the Thermoflex/Peace[®] environment [28]. To accurately describe the plant operation at any load, reliable plant data about the design features and operation of the main components are used to validate the plant parameters and to compare the efficiency and other performance. The characteristic curves of the single components (steam turbines, HRSG) are also “extracted” from the results to have a direct information about their possible behavior when solar energy is added and, in turn, further improve the understanding of the off-design control philosophy of the total system.

2.1. Power output validation

After calibration with real plant data at nominal load (continuous nominal load, CNC), the off-design model is run at different loads (CMA: minimum load to keep gas turbine emissions below environmental limits; CCT: minimum load to keep steam superheating and reheating temperatures at nominal values; CMT: minimum load to preserve the equipment). Model predictions (dotted violet lines) are compared with real plant data (solid blue lines) in Fig. 1. Both gas turbine and steam turbine power output are well predicted at any load, being the maximum deviation lower than 4%.

2.2. Gas turbine

The control philosophy of the gas turbine varies depending on load:

- At loads between 100% and 50% (CMA and CCT) the gas turbine control system adjusts the pitch angle of the variable guide vanes at compressor inlet (VGV) to reduce the passage area for the decreased air mass flow rate and simultaneously adjusts fuel input to keep the turbine outlet temperature (*TOT*) constant. The decrease of exhaust mass flow rate (m_{EXG}) is accompanied by a pressure drop at turbine inlet and, in turn, of pressure ratio (*PR*). For a constant *TOT* and reduced *PR* the turbine inlet temperature (*TIT*) decreases. Due to the combined effect of reduced *PR* and reduced *TIT* also the cycle efficiency (η) decreases.
- At loads lower than 50% (CMT) the VGV are fully closed and the air mass flow rate is constant. Fuel input is adjusted to reduce *TIT*. Both *TOT* and *PR* decrease. The cycle efficiency markedly decreases.

Figs. 2 and 3 show the gas turbine parameters predicted by the off-design model.

2.3. Steam cycle

The bottoming steam cycle follows the load variations of the gas turbine as described in the following sections.

2.3.1. Cycle parameters

At reduced loads the steam mass flow rate (Fig. 4a) and turbine inlet pressure (Fig. 4b) decrease due to the lower energy content associated with the gas turbine exhaust gases. Fig. 4 shows good agreement between model predictions and real plant data for all loads except the minimum (CMT) where a lower amount of HP

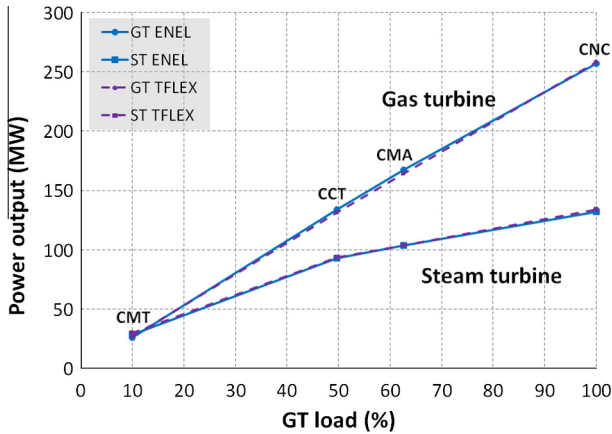


Fig. 1. Gas turbine and steam turbine power output versus gas turbine load. Comparison between plant data (solid blue lines) and Thermoflex® predictions (violet dotted lines). (For interpretation of the references to colour in this figure legend, the reader is referred to the web version of this article.)

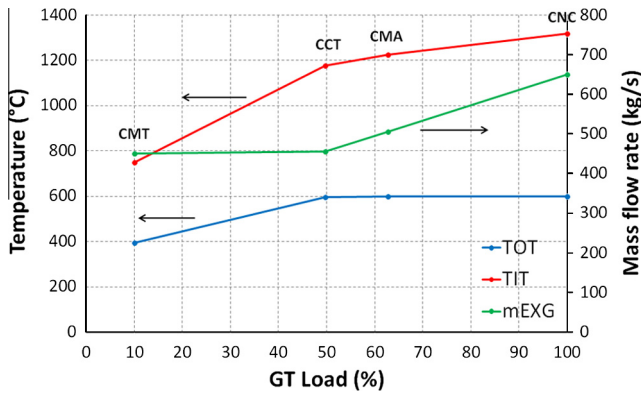


Fig. 2. Thermoflex® results: variation of turbine outlet temperature (TOT), turbine inlet temperature (TIT) and exhaust gas mass flow rate (m_{EXG}) with gas turbine load.

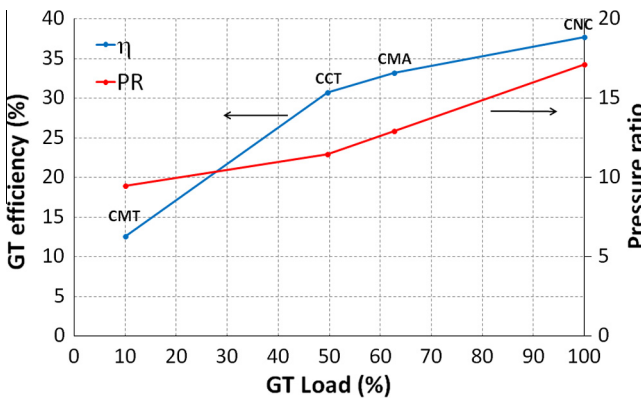


Fig. 3. Thermoflex® results: variation of gas turbine pressure ratio (PR) and cycle efficiency (η) with gas turbine load.

steam is generated at higher pressures (50 bar vs 28 bar) in the real plant.

2.3.2. Steam turbines characteristic curves

The steam turbines efficiencies at nominal load (CNC) are calculated to match the power output of the real plant (i.e., ENEL data). The calculated isentropic efficiencies are 82.74%, 85.12% and 86.36% for the high pressure turbine (HPT), intermediate pressure

turbine (IPT) and low pressure turbine (LPT), respectively. At off-design conditions the relationship steam mass flow rate – turbine inlet pressure – turbine inlet temperature for a generic expansion ratio (p_{out}/p_{in}) is given by the “ellipse law”:

$$\frac{\dot{m}\sqrt{T_{in}}}{p_{in}} \Big|_{ST} = \sqrt{\frac{1 - \left(\frac{p_{out}}{p_{in}}\right)^2}{1 - \left(\frac{p_{out}}{p_{in}}\right)^2_D}} \quad (1)$$

where the subscript “D” refers to the design point parameters. From Eq. (1) the mass flow rate of steam through the turbine can be directly calculated from the turbine inlet temperature and inlet pressure at any load. The steam turbine efficiencies vary with the “flow function” $\phi = \frac{\dot{m}\sqrt{T_{in}}}{p_{in}}$ (also called “corrected mass flow rate”, m_{corr}) according to a Thermoflex® built-in correlation in the form:

$$\eta = \eta_D - f\left(\frac{\phi}{\phi_D}\right) \quad (2)$$

Fig. 5a and b show the relationship between expansion ratio and corrected mass flow rate for the IP and HP steam turbines respectively. The operating points lie along an ellipse in the “expansion ratio-corrected mass flow rate” plane. While the corrected mass flow rate in the HP turbine is approximately constant at any load, the rather low expansion ratios in the IP turbine result in a significant variation of the corrected mass flow rate and, accordingly, of the turbine isentropic efficiency which decreases from 85.1% at nominal load (CNC) down to 75.0% at minimum load (CMT).

2.3.3. Heat recovery steam generator

The geometrical data for all tube banks of the HRSG are included in Thermoflex® to model the real geometry of the HRSG.

For each tube bank the heat transfer in the HRSG is given by:

$$q = U \cdot A \cdot LMTD \quad (3)$$

At off-design the reduced exhaust gas and steam mass flow rates result in a decrease of q and U . Fig. 6a shows the reduction of the heat duty compared to the nominal heat duty (i.e., q/q_D) for all the HRSG banks and at any load. Similarly, Fig. 6b shows the reduction of the overall heat transfer coefficient from the nominal value (i.e., U/U_D). It can be easily noticed that q decreases more than U at reduced loads. Accordingly, the LMTDs and minimum temperature differences ΔT_{min} (Fig. 6c) decrease at reduced loads. At the minimum load (CMT) ΔT_{min} becomes very small (close to 1 °C or even lower) in the HP economizers and HP evaporator.

2.4. Combined cycle

Fig. 7 shows the thermal efficiency predictions for the topping, bottoming and combined cycles. Two different trends can be distinguished:

- At gas turbine loads between 100% and 50% the steam cycle efficiency is approximately constant because the steam temperatures at turbine inlets are close to the design values and the reduction of steam pressure has only a minor impact on performance. So, the trend of combined cycle efficiency follows the trend of gas turbine efficiency.
- At gas turbine loads lower than 50% the steam cycle efficiency decreases due to the lower temperatures at the inlet of steam turbines compared to the design value. The thermal efficiency of the combined cycle markedly decreases due to the concurrent decrease of both topping and bottoming cycle thermal efficiencies.

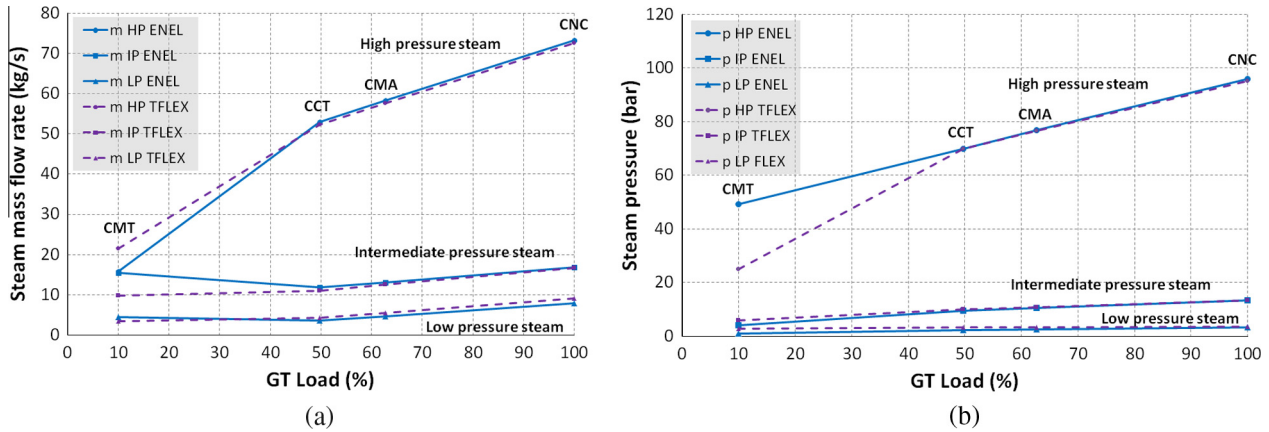


Fig. 4. Variation of HP, IP and LP (a) steam mass flow rate and (b) evaporation pressure with gas turbine load. Comparison between plant data (solid blue lines) and Thermoflex[®] predictions (violet dotted lines). (For interpretation of the references to colour in this figure legend, the reader is referred to the web version of this article.)

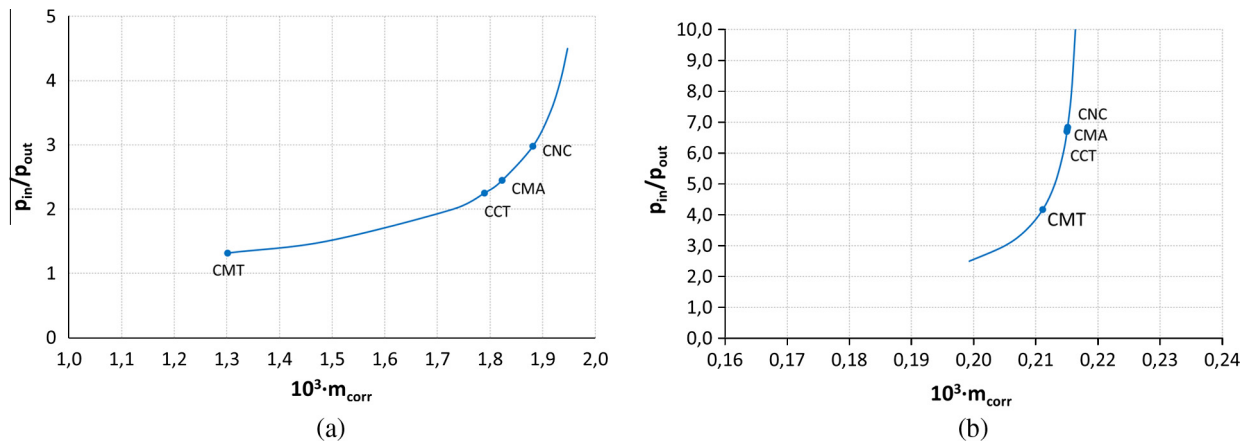


Fig. 5. Relationship between expansion ratio and corrected mass flow rate for the (a) IP steam turbine and (b) HP steam turbine.

As shown in Table 1, the calculated efficiencies of the combined cycle are consistent with the real plant data (provided by ENEL), being the difference lower than 1% at all loads but CMT. At CMT the simulation model underestimates by 9% the thermal efficiency of the combined cycle.

3. Operating strategies and design modifications of integrated solar combined cycles

The optimum integration of concentrated solar energy in the bottoming cycle is studied here starting from the off-design model of the natural gas combined cycle described in Section 2. The selected integrated solar combined cycle configuration (named in the following ISCC1) includes a parabolic trough solar field having thermal oil as heat transfer fluid (Therminol VP-1) and a solar steam generator where a fraction of saturated water is evaporated and sent to the HRSG for superheating. This layout provided the highest solar-to-electrical efficiency among several hybrid layouts in the thermodynamic analysis carried out at design conditions in [29], and was therefore selected for this study. Fig. 8 shows the Thermoflex[®] flowsheet of ISCC1.

3.1. Power boosting vs fuel saving

Two different strategies for integration of solar energy into the reference NGCC are considered:

- “Power Boosting” operation consists in the addition of the solar input to the reference combined cycle at constant (reference) fuel input.
- “Fuel Saving” operation consists in the generation of some power from solar energy in substitution of the same power in the reference combined cycle, to reduce total fuel consumption.

In power boosting mode the gas turbine operates at nominal load (100%) with the highest thermal efficiency whereas in fuel saving mode the reduction of the gas turbine load results in a lower thermal efficiency. On the other hand, power boosting may require new and larger equipment in the steam bottoming cycle (e.g., HRSG, steam turbines) whereas fuel saving may potentially use most of the existing equipment (objective not always fulfilled). Thus, both strategies are analyzed in the following in the search for optimum integration of solar energy in the combined cycle.

3.2. Performance metrics

The following metrics are considered to evaluate plant performance:

- Incremental solar radiation-to-electrical efficiency:

$$\eta_{incr_solar1} = \frac{\Delta \dot{W}_{ST}}{ANI \cdot A_{coll}} \quad (4)$$

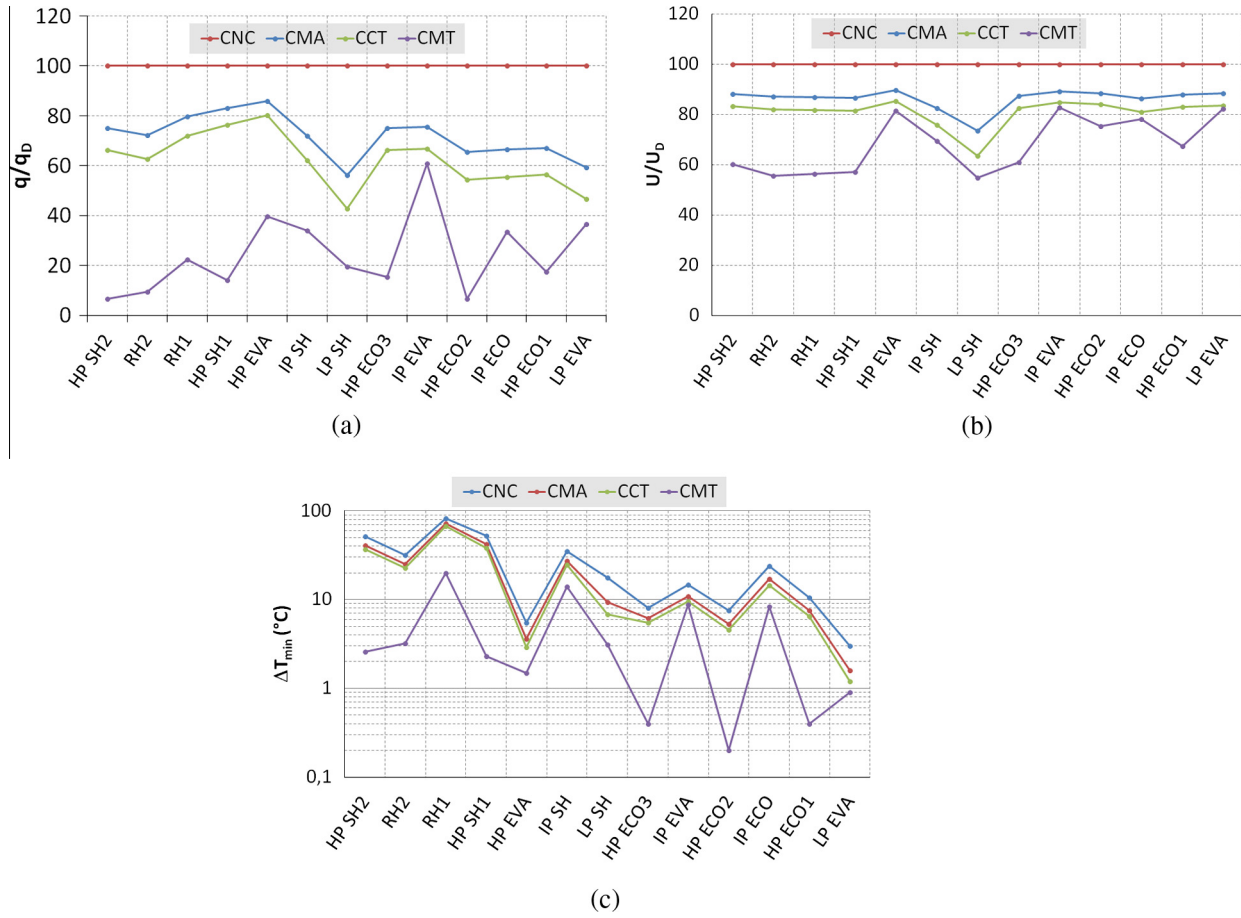


Fig. 6. Variation at different gas turbine loads of (a) HRSG heat duties; (b) overall heat transfer coefficients; (c) minimum temperature difference.

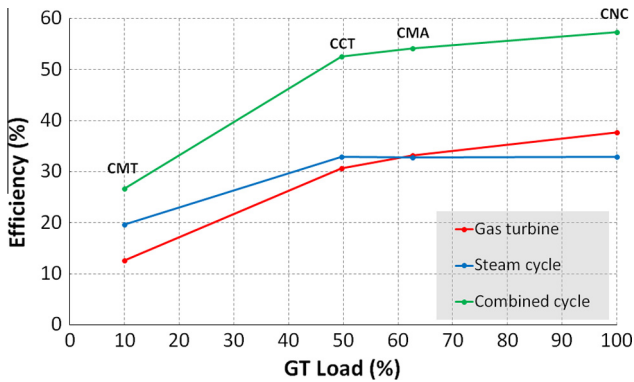


Fig. 7. Thermoflex® results: variation of gas turbine, steam cycle and combined cycle thermal efficiency with gas turbine load.

where $\Delta \dot{W}_{ST}$ is the power output increase of the steam bottoming cycle, ANI is the aperture normal irradiance and A_{coll} the solar collector area.

- Incremental solar thermal-to-electrical efficiency:

$$\eta_{incr_solar2} = \frac{\Delta \dot{W}_{ST}}{Q_{th,sol}} \quad (5)$$

where $Q_{th,sol}$ is the solar thermal power.

- Solar field efficiency:

$$\eta_{solar_field} = \frac{\dot{Q}_{th,sol}}{ANI \cdot A_{coll}} \quad (6)$$

- ISCC thermal efficiency:

$$\eta_{ISCC} = \frac{\dot{W}_{ISCC}}{\dot{Q}_{fuel} + ANI \cdot A_{coll}} \quad (7)$$

where \dot{W}_{ISCC} is the power output of the integrated solar combined cycle and \dot{Q}_{fuel} is the natural gas input.

Note that in the fuel saving scenario the definitions of solar-to-electrical efficiencies (Eqs. (3) and (4)) include at the numerator the incremental power output from solar compared to the reference NGCC running at reduced loads, while the ISCC efficiency (Eq. (6)) include at the denominator the natural gas input at reduced gas turbine loads.

3.3. Power boosting strategy

Three scenarios (PB1, PB2, PB3) are considered in the power boosting operation of ISCC1:

- In PB1 the main equipment of the reference NGCC is kept unchanged.
- In PB2 a larger steam turbine is included.
- In PB3 both a larger steam turbine and additional tube banks in the HRSG are included.

In all scenarios the reference gas turbine operates at nominal load (100%). Fig. 9 shows a simplified layout of ISCC1 (referring to a single pressure level system) with the only purpose of high-

Table 1
Combined cycle off-design thermal efficiency. Comparison between plant data (ENEL data) and Thermoflex® predictions.

Load	Thermoflex® results				ENEL data				Difference (%)			
	CNC	CMA	CCT	CMT	CNC	CMA	CCT	CMT	CNC	CMA	CCT	CMT
η_{cc}	57.32	54.20	52.52	26.69	56.98	54.51	52.86	29.35	+0.59	-0.57	-0.63	-9.07

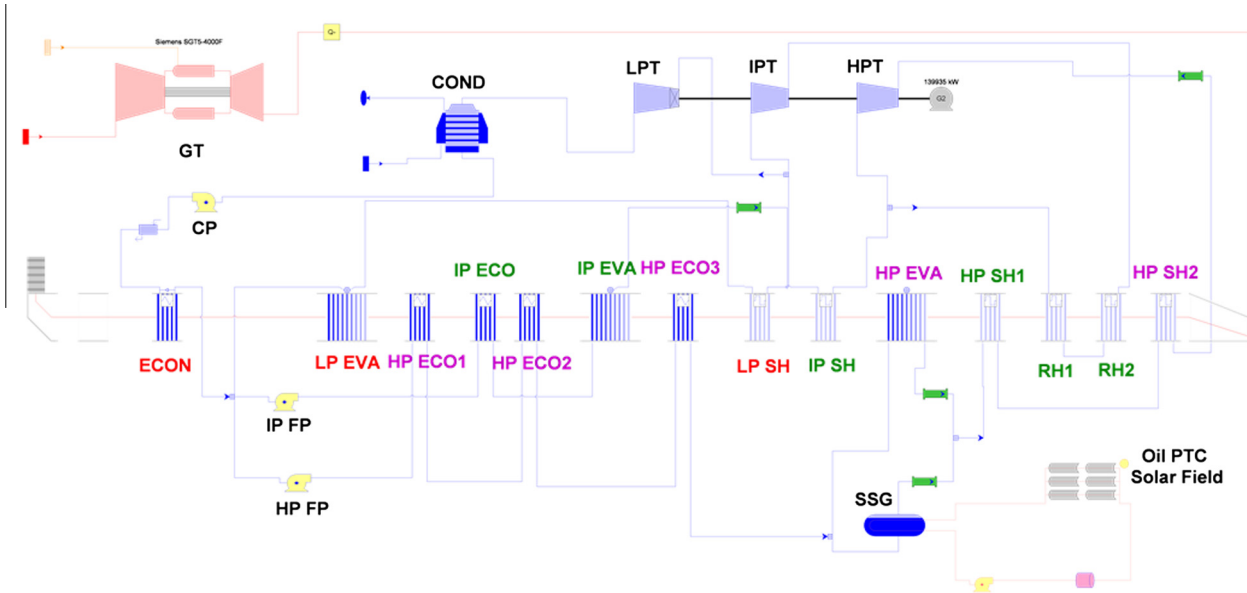


Fig. 8. Thermoflex® flowsheet of the integrated solar combined cycle (ISCC1).

lighting the integration points between HRSG and solar section and the modifications (in red color¹) to the reference NGCC equipment.

3.3.1. First power boosting scenario (PB1)

In PB1 the combined cycle section of the ISCC includes the same equipment of the reference NGCC. The gas turbine operates at nominal load (100%) whereas the steam turbines and HRSG operate at off-design due to the increased steam mass flow rate raised from solar energy. The power output of the steam bottoming cycle increases from 134.0 MW_e (i.e., the power output in the reference NGCC) up to a maximum of 150.9 MW_e (achieved with a solar steam mass flow rate equal to 30 kg/s). The incremental power output from solar (16.9 MW_e) is limited by the achievement of the maximum allowed steam pressure (124.2 bar) in the HRSG tubes. The solar collectors area required to boost the power by 16.9 MW_e at the design aperture normal irradiance (850 W/m²) is 77,435 m². Fig. 10 shows the increase of steam mass flow rate (blue line) and pressure (violet line) at the inlet of HP turbine resulting from the increase of steam mass flow rate generated from solar. The increase of steam mass flow rate is accompanied by an increase of steam pressure at turbine inlet being the “corrected mass flow rate” approximately constant (as shown in Fig. 5a).

The steam temperatures at the outlet of superheater (i.e., inlet of HPT) and reheat (i.e., inlet of IPT) decrease from the design value (≈540 °C) due to the increase of steam mass flow rate, being the HRSG tube banks area equal to that of the reference NGCC. When the steam generated from solar is maximum (30 kg/s), the steam temperatures at the inlet of HPT and IPT are 510 and 518 °C, respectively. The incremental solar radiation-to-electrical

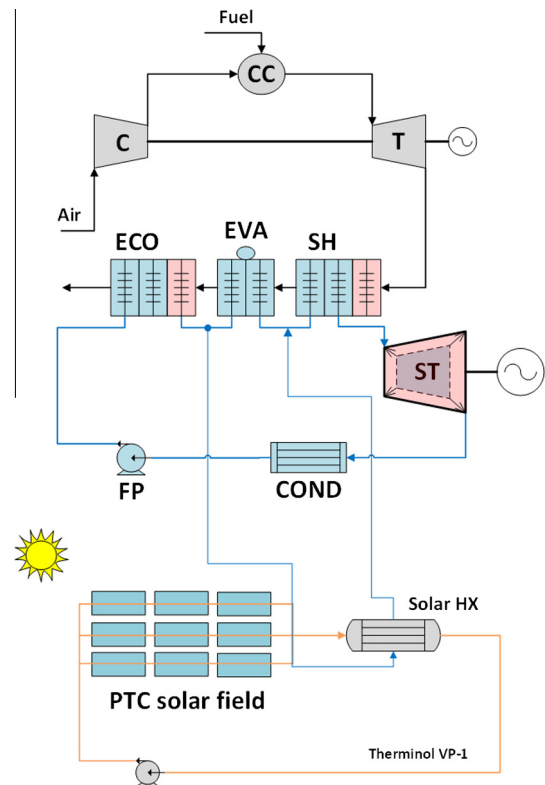


Fig. 9. Schematic layout of ISCC1.

¹ For interpretation of color in Figs. 9, 10, 12, 14, 15, 17, the reader is referred to the web version of this article.

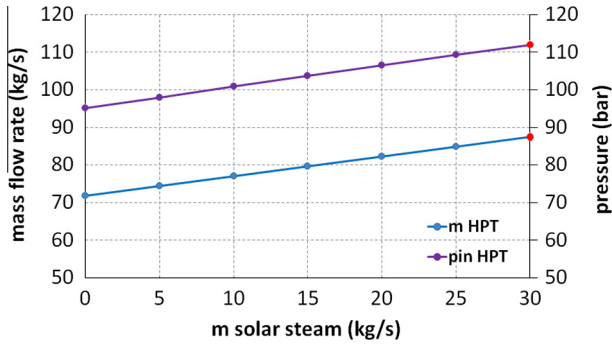


Fig. 10. Steam mass flow rate and pressure at the inlet of HPT in PB1.

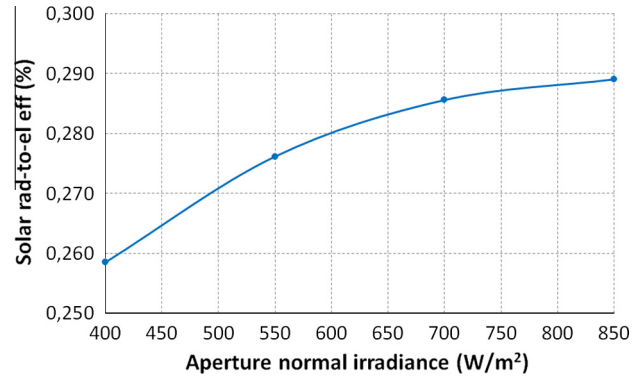


Fig. 11. Variation of solar radiation-to-electrical efficiency in PB3.

efficiency (η_{incr_solar1}) reaches 26.1–27.1% whereas the incremental solar thermal-to-electrical efficiency (η_{incr_solar2}) assumes values between 43.6% and 44.8%, depending on the amount of steam generated from solar. The calculated values are consistent with those reported in the literature when solar integration on the HP level is considered. The solar efficiencies slightly decrease with the increase of steam mass flow rate generated from solar due to lower steam temperatures at HPT and IPT inlet (fixed HRSG design) and the slight decrease of turbine isentropic efficiencies from the design values.

3.3.2. Second power boosting scenario (PB2)

In PB2 the bottoming cycle in the ISCC includes larger steam turbines than in the reference NGCC but keeps the original HRSG. The solar field and steam turbines are designed for a power boost of 50 MW_e (at the design irradiance of 850 W/m²) which asks for a parabolic trough collectors area of 246,120 m² and a steam mass flow rate generated from solar equal to 90 kg/s. With solar addition the power output of the bottoming cycle increases from 134.0 MW_e up to 184.6 MW_e. The steam temperatures at the inlet of HPT (453 °C) and IPT (476 °C) are much lower than 540 °C because of the higher steam mass flow rates compared to reference NGCC, being the area of the HRSG unaltered. In PB2 the turbines are designed for such modified steam conditions (higher mass flow rates and lower steam temperatures). Although this scenario enables to meet the +50 MW_e target, it yields quite low solar radiation and solar thermal-to-electrical efficiencies (24.2% and 39.3%, respectively at the nominal solar irradiance) due to the moderate steam temperatures at HPT and IPT inlets. The efficiencies of the steam turbines decrease only slightly (less than 0.5%) when the solar irradiance is reduced because the flow function remains approximately constant.

3.3.3. Third power boosting scenario (PB3)

In PB3 the bottoming steam cycle includes, besides the larger steam turbines, a larger HRSG compared to the reference NGCC. In particular, the surface area of the high pressure economizers (HP ECO1–2–3), superheaters (HP SH1–2) and reheaters (RH1–2) is doubled. Similarly to PB2 the solar field is designed to supply +50 MW_e at the design irradiance (ANI) of 850 W/m². In this new layout (PB3) a steam mass flow rate generated from solar equal to 80 kg/s (i.e., 10 kg/s less than in PB2) is needed to boost the power output by approximately 50 MW_e. The required parabolic trough collectors area is 206,040 m² which is 16.3% lower than that required in PB2 scenario. With solar steam addition the power output of the steam cycle increases from 134.0 MW_e up to 184.6 MW_e. Despite the enlarged HRSG design the steam temperatures at the inlet of HPT and IPT are still about 20 °C lower than 540 °C at the design ANI (850 W/m²), whereas they slightly exceed 540 °C at reduced ANIs. Similarly to PB2, in PB3 the turbines are specifically

Table 2 Comparison of power boosting scenarios.

Scenario	PB1	PB2	PB3
Retrofit (new equipment)	None	Steam turbines	Steam turbines and HRSG
Power output increase (MW)	+16.9 (max)	+50.5	+50.6
Collectors area (m ²)	77,435	246,120	206,040
Solar radiation-to-electrical efficiency (%)	26.1	24.2	28.9
Solar thermal-to-electrical efficiency (%)	43.6	39.3	47.0
η_{ISCC} (%)	54.6	49.6	51.4

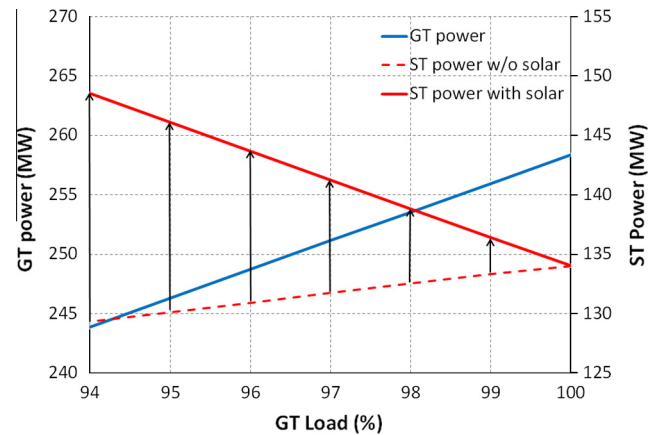


Fig. 12. Variation with GT load of the power output of GT cycle and steam bottoming cycle with and without hybridization in FS1.

designed for such steam conditions. The maximum solar radiation-to-electrical efficiency (28.9%) is the highest among the power boosting scenarios considered (Fig. 11) and the solar thermal-to-electrical efficiency reaches approximately 47% at any ANI.

3.3.4. Comparison of power boosting scenarios

Table 2 compares features and performance of the power boosting scenarios at ANI = 850 W/m². PB1 does not need design modifications compared to the NGCC but does not meet the 50 MW_e target. PB2 and PB3 both meet the 50 MW_e target but require new equipment. The higher solar efficiencies achieved by PB3 result in a smaller collectors area (and costs) than PB2. The ISCC thermal efficiency is higher in PB3 which means a better utilization of both fuel energy and solar energy compared to PB2. Note

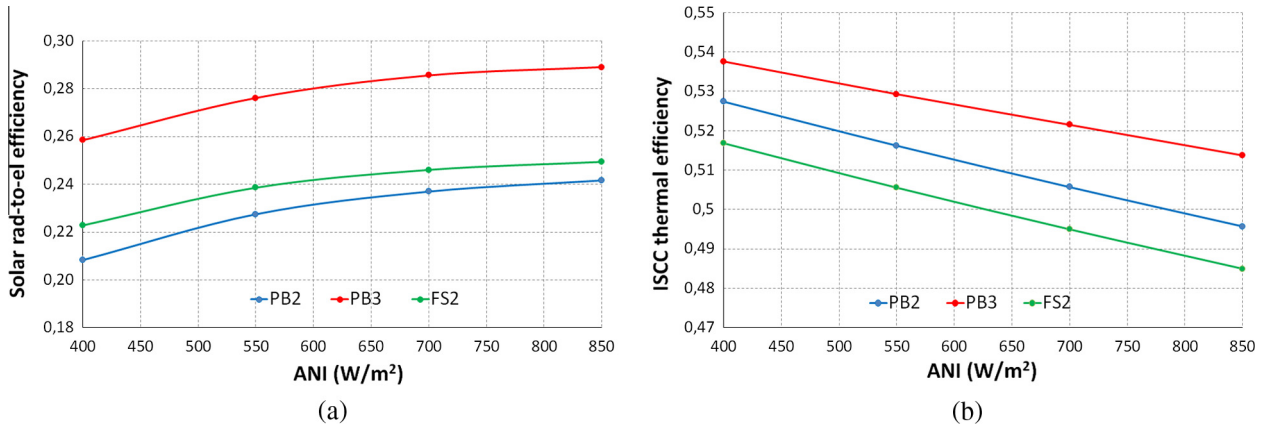


Fig. 13. (a) Solar radiation-to-electrical efficiency versus ANI; (b) thermal efficiency of ISCC versus ANI.

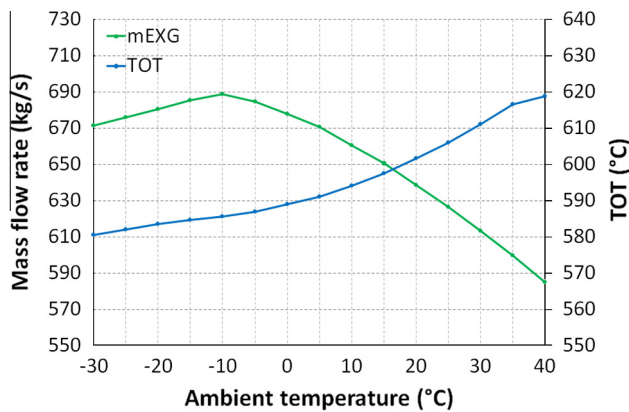


Fig. 14. Gas turbine exhausts mass flow rate (m_{EXG}) and outlet temperature (TOT) versus ambient temperature.

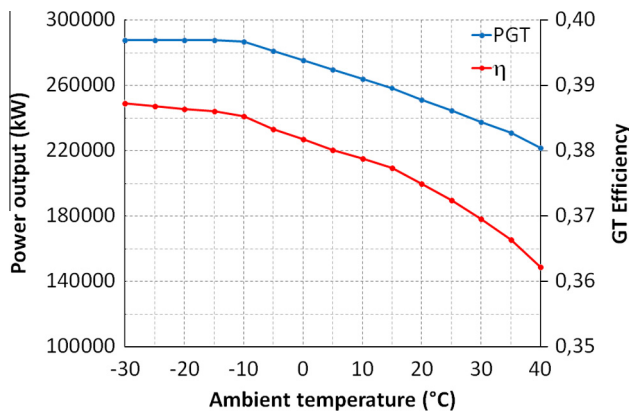


Fig. 15. Gas turbine power output (P_{GT}) and thermal efficiency (η) versus ambient temperature.

that an even comparison of η_{ISCC} between PB1 and PB2–PB3 is not possible being the former advantaged by the lower solar share.

From Table 2, PB3 appears as the most efficient scenario to obtain a 50 MW_e power output increase because of the smaller collectors area and higher ISCC thermal efficiency. However, PB3 requires the greatest modifications to the reference combined cycle. On the other hand, PB1 allows power output to be increased up to a maximum of 16.9 MW_e while reaching fairly high solar efficiencies and keeping the existing plant infrastructure. Accordingly, PB1 will be further investigated in Section 4.

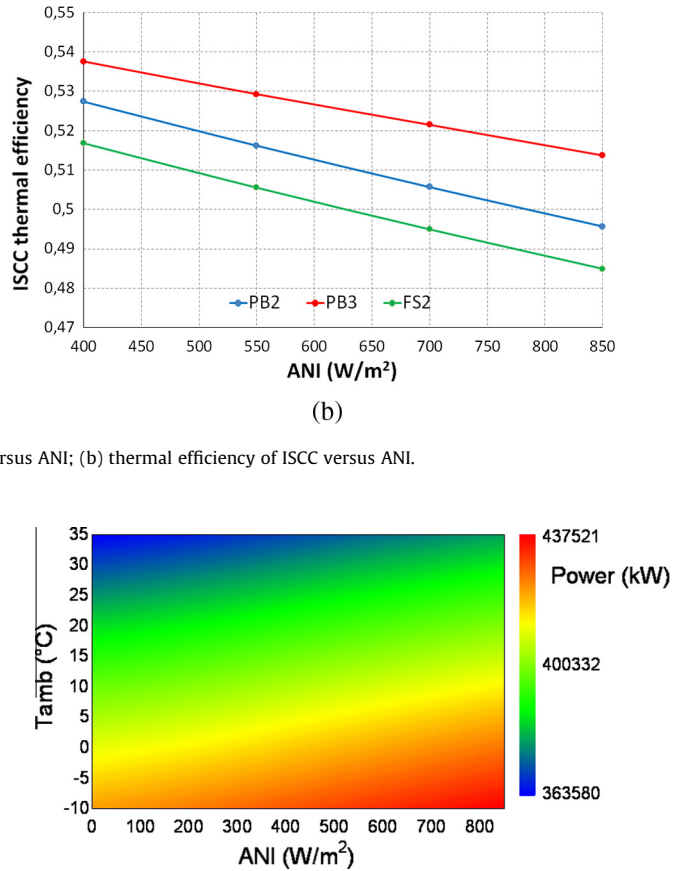


Fig. 16. Variation of ISCC1 power output with ambient temperature and incident irradiance.

3.4. Fuel saving strategy

Two scenarios (FS1 and FS2) are considered in the fuel saving operation of ISCC1: in FS1 all the equipment of the reference NGCC is kept unchanged; in FS2 larger steam turbines are included whereas the HRSG is kept unchanged. In both scenarios the gas turbine runs at reduced loads.

3.4.1. First fuel saving scenario (FS1)

In FS1 the combined cycle section of ISCC1 includes the same equipment of the reference combined cycle. The gas turbine operates at reduced loads (in the interval 94–100%) to reduce natural gas consumption. Solar fields with different sizes are designed to fill the power output drop of the combined cycle at reduced GT loads in order to keep the overall power output constant. Fig. 12 shows the decrease of gas turbine (solid blue line) and steam cycle power output (red dotted line) at reduced GT loads. The incremental power output from solar makes up for both the power output drops. Solar input increases the power output of the bottoming steam cycle (solid red line in Fig. 12) in order to meet a constant power output of the ISCC equal to the power output of the reference NGCC at full load. The decrease of gas turbine efficiency is 0.5%-points when moving from 100% to 94% GT load.

The maximum power output from solar (+19.3 MW_e) is limited by the maximum allowed steam pressure (124.2 bar) in the tubes. At these conditions the GT load is 94%, the steam mass flow rate evaporated from solar amounts to 33.4 kg/s and the required solar collector area is 83,600 m^2 . The maximum incremental power output from solar (before reaching the maximum pressure) is higher than in PB1 (19.3 vs 16.9 MW_e) and also the solar radiation-to-

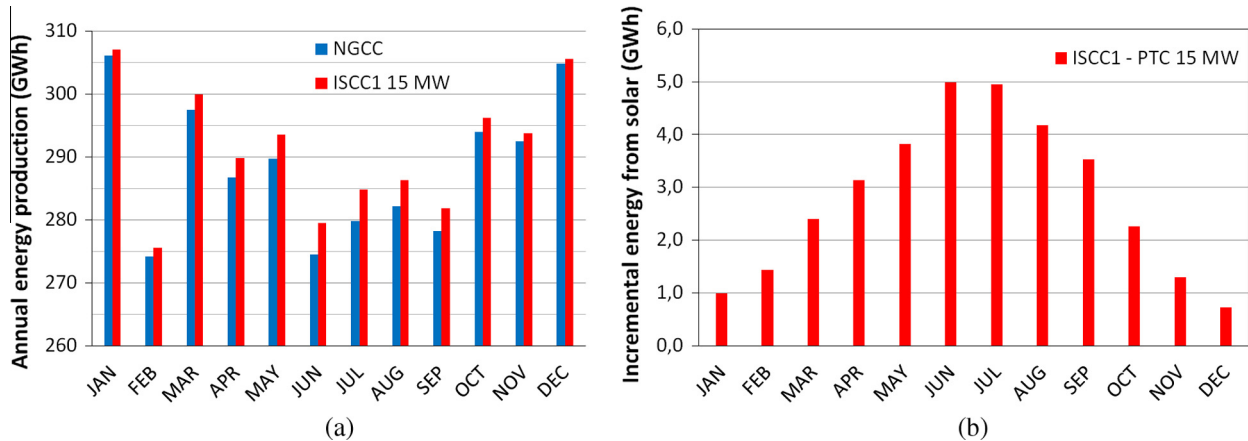


Fig. 17. (a) Monthly energy production of NGCC and ISCC1 in Fallon (NV, USA); (b) monthly solar incremental energy production of ISCC1 in Fallon (NV, USA).

electrical efficiency (27.1–27.6%) is slightly higher than in PB1 (26.1–27.1%).

3.4.2. Second fuel saving scenario (FS2)

In FS2 the bottoming cycle in the ISCC includes larger steam turbines to fulfill the +50 MW_e target from solar whereas the HRSG design is the same as in the reference NGCC to minimize the modifications to the existing equipment. The gas turbine operates at the reduced load of 84.5% which entails a power output reduction of the combined cycle equal to 50 MW_e. At such reduced load the gas turbine power output reduction is 37.8 MW_e, the gas turbine efficiency is 1.5%-points lower than the efficiency at 100% load (36.2% vs 37.7%) and the power output reduction of the steam cycle is 12.4 MW_e (i.e., from 134.0 MW_e to 121.6 MW_e). The solar field design to supply the missing 50 MW_e requires a solar collectors area of 235,430 m² at 850 W/m². The steam outlet temperatures from superheater (457 °C) and reheater (476 °C) are much lower than 540 °C, at medium-high ANI, being the HRSG identical to that in the NGCC. Thus, similarly to PB2, the resulting solar radiation-to-electrical efficiency is quite low (24.9%).

3.5. Comparison between fuel saving and power boosting

Fig. 13 shows the variation of solar radiation-to-electrical efficiency (Fig. 13a) and ISCC thermal efficiency (Fig. 13b) versus solar irradiance (ANI) only for those scenarios fulfilling the +50 MW_e target (i.e., PB2, PB3 and FS2). PB3 yields the highest solar radiation-to-electrical efficiency at any ANI but requires both larger steam turbines and larger HRSG. FS2 yields intermediate solar radiation-to-electrical efficiency, slightly higher than PB2 (both requiring a new steam turbine). The highest ISCC thermal efficiency is achieved by PB3 whereas the lowest by FS2 due to the lower gas turbine efficiency (operation at reduced load) and steam cycle efficiency (low steam temperatures at turbines inlets).

4. Maximum annual energy production of ISCC using the same equipment of the original NGCC

In this section the PB1 scenario is selected for further analysis since it does not require modifications to the equipment of the NGCC and yields relatively high solar-to-electrical and ISCC efficiencies. The aim is the evaluation of the annual solar share attainable by retrofitting a NGCC with solar energy without modifying the existing equipment. For this purpose, the variation of gas turbine parameters with ambient temperature is firstly evaluated (while ISO conditions are assumed for ambient pressure and

humidity). Afterwards, both ambient temperature and solar irradiance are modified in the ISCC model to get a map of power output versus ambient conditions. This map is used to calculate the overall energy production and incremental energy production from solar in a given location (Fallon, NV) with high levels of solar irradiation.

4.1. Variation of gas turbine parameters with ambient temperature

Ambient temperature markedly affects the operation of the gas turbine. The variation of the main gas turbine parameters in a wide range of ambient temperatures between –30 °C and 40 °C is shown in Figs. 14 and 15 to illustrate the control philosophy of the gas turbine Siemens SGT5-4000F as predicted by Thermoflex®.

The volumetric flow rate at compressor inlet is constant ($V_{in,c} = \text{cost}$), so the mass flow rate of air and exhaust gases (green line in Fig. 14) decrease at high ambient temperatures due the reduction of air density with temperature ($p/\rho = RT$). On the other hand, the turbine outlet temperature (blue line in Fig. 14) increases at high ambient temperatures due to the lower pressure ratio and constant TIT . The gas turbine pressure ratio decreases at high ambient temperatures because of the lower mass flow rate of exhaust gases, according to:

$$\frac{\dot{m}_{EXG} \sqrt{T_{in}}}{p_{in}} \approx \text{cost} \quad (8)$$

where T_{in} and p_{in} are the temperature and pressure at gas turbine inlet. The turbine inlet temperature is approximately constant (1320 °C) in the range of ambient temperatures between –10 °C and 35 °C. The gas turbine power output (blue line in Fig. 15) markedly decreases at high ambient temperatures due to the reduction of exhausts mass flow rate and pressure ratio. At very low ambient temperatures (<–10 °C) the power output is limited to a maximum value of 287.9 MW_e. The gas turbine thermal efficiency decreases at high ambient temperatures due to the lower net specific work.

4.2. Variation of ISCC power output with ambient temperature and solar irradiance

The solar field is sized in PB1 to provide an incremental power output of 15 MW_e from solar at the nominal incident direct irradiance of 850 W/m². This value is 1.9 MW_e lower than the maximum incremental power output of 16.9 MW_e (Section 3.3.1) to keep a safety margin from the maximum allowable steam pressure. The required parabolic trough solar collectors area is 66,110 m². Fig. 16 shows the variation of ISCC power output with ambient temperature and incident irradiance in PB1. The power output

Table 3
Economic evaluation of power boosting scenarios.

	HRSG (M\$)	Steam turbines (M\$)	Solar field (M\$)	Incr. investment (M\$)
NGCC	13.64	17.44	/	/
ISCC PB1	13.64	17.44	39.67	39.67
ISCC PB2	13.64	24.03	147.67	154.26
ISCC PB3	21.25	24.03	123.62	137.82

markedly increases at low ambient temperatures due to the high impact of this temperature on gas turbine power. On the other hand, it only slightly increases at high irradiation levels due to the low solar share in PB1.

The annual energy production is evaluated considering the site of Fallon in Nevada (USA) having high levels of direct normal irradiation. In Fallon the annual direct solar irradiation is 2480 kW h/m² year and the average annual temperature is 12.2 °C. For this site historical hourly data (8760 data) are available for both ambient temperature and direct normal irradiation (DNI). The calculated annual energy production (assuming 100% availability) is 3460.3 GW h for the NGCC and 3494.0 GW h for the ISCC, which represents an annual energy increase from solar equal to 33.7 GW h and a solar share of approximately 1%. Fig. 17 shows the comparison between the monthly energy production of the reference NGCC (blue bars) and ISCC (red bars).

4.3. Economic evaluation

A preliminary economic analysis is carried out using the following assumptions. Installed cost of the HRSG sections [30]: economizer: 45.70 \$/m²; evaporator: 34.80 \$/m²; superheater: 96.20 \$/m². Unit cost of a steam turbine: 130 \$/kW [31]. Installed cost of the parabolic trough solar field: 600 \$/m² [28]. The costs are updated using the 2014 chemical engineering plant cost index (CEPCI = 576.1). The calculated costs in million \$ are shown in Table 3 for the reference NGCC and the three power boosting scenarios.

Assuming a capital recovery factor [32] equal to 0.10 and a maintenance and repairs cost equal to 2% of the capital investment, the incremental LCOE calculated for PB1 is 14.1 c\$/kW h.

5. Conclusions

The off-design model of the reference natural gas combined cycle developed in this study provides an accurate prediction of the gas turbine and steam cycle thermodynamic parameters and power output at any load. The difference between model predictions and real plant data are limited within few percentage points, with highest deviations observed only at the lowest load (10%) which is of low significance for this analysis.

The maximum power output increment from solar energy using the same equipment of the reference natural gas combined cycle is limited to approximately 17 MW_e due to a mechanical limitation on the maximum allowed steam pressure in the tubes. Accordingly, some modifications to the existing equipment are needed to increase the solar share and meet the +50 MW_e target. In particular, a larger steam turbine specifically designed to swallow the increased steam mass flow rate allows the target to be achieved, but at a moderate incremental solar radiation-to-electrical efficiency (24.2%). The inclusion of a larger heat recovery steam generator (combined with a larger steam turbine) enables higher steam temperatures at turbines inlet and, in turn, improves this efficiency up to 29%.

The fuel saving operation has shown that the maximum power output from solar energy using the same equipment of the refer-

ence natural gas combined cycle is 19 MW_e (i.e., approximately 2 MW_e higher than using the power boosting strategy). Thus, similarly to power boosting also fuel saving operation asks for a larger steam turbine to meet the +50 MW_e target. On the other hand, the overall plant efficiency (48.5%) is 1.1%-point lower due to the lower thermal efficiency of the gas turbine at reduced loads.

So, regardless of the operational strategy, the addition of 50 MW_e from solar within a 390 MW_e combined cycle needs a significant modification to the equipment of the bottoming steam cycle. Steam turbines with increased swallowing capacity are needed to assure the technical feasibility of the ISCC system, and extended heat transfer surface areas in the HRSG are required to obtain higher solar-to-electrical and ISCC efficiencies. Was the +50 MW_e target from solar not binding, a viable ISCC plant could be obtained by using the same equipment of the original natural gas combined cycle with the only addition of the solar field. In such conditions the solar radiation-to-electrical efficiency would approach 27%, which is remarkable and higher than that achievable in solar thermal power plants, and the incremental solar levelized cost of electricity would be around 14.1 c\$/kW h. The only drawback is the limited solar share achievable, approximately 1% of the annual electricity production by the overall plant, which is not enough to fill the power output reduction during the warm season and to level the monthly energy production profile.

Acknowledgements

The work was supported by ENEL in the framework of a wider research interest on the development of new ISCC technologies. Alessio Bardi, Marco Paci, Stefano Sigali and Nicola Rossi of ENEL Engineering and Innovation are gratefully acknowledged for helpful suggestions and discussions. Special thanks go to Prof. Andrea Lazzaretto and Dr. Sergio Rech of University of Padova for their valuable support during the research.

References

- [1] Behar O, Khellaf A, Mohammadi K, Ait-Kaci S. A review of integrated solar combined cycle system (ISCCS) with a parabolic trough technology. *Renew Sust Energy Rev* 2014;39:223–50.
- [2] Jamel MS, Rahman AA, Shamsuddin AH. Advances in the integration of solar thermal energy with conventional and non-conventional power plants. *Renew Sust Energy Rev* 2013;20:71–81.
- [3] Audinet P, März T. Lessons for solar power development from the world's first integrated solar combined cycle project. In: *Proceeding of SolarPACES2011, Concentrating solar power and chemical energy systems*; 2011 September 20–23; Granada, Spain.
- [4] Allani Y, Favrat D, von Spakovsky MR. CO₂ mitigation through the use of hybrid solar-combined cycles. *Energy Convers Manage* 1997;38:661–7.
- [5] Kelly B, Herrmann U, Hale MJ. Optimization studies for integrated solar combined cycle systems. In: *Proceedings of solar forum 2001, solar energy: the power to choose*; 2001 April 21–25, Washington DC, USA.
- [6] Rovira A, Montes MJ, Varela F, Gil M. Comparison of heat transfer fluid and direct steam generation technologies for integrated solar combined cycles. *Appl Therm Eng* 2013;52:264–74.
- [7] Li Y, Yang Y. Thermodynamic analysis of a novel integrated solar combined cycle. *Appl Energy* 2014;122:133–42.
- [8] Montes MJ, Rovira A, Muñoz M, Martínez-Val JM. Performance analysis of an integrated solar combined cycle using direct steam generation in parabolic trough collectors. *Appl Energy* 2011;88:3228–38.

- [9] Baghernejad A, Yaghoubi M. Exergoeconomic analysis and optimization of an integrated solar combined cycle system (ISCCS) using genetic algorithm. *Energy Convers Manage* 2011;52:2193–203.
- [10] Libby C, Golden J, Bedilion R, Turchi C. Assessment of direct steam generation technologies for solar thermal augmented steam cycle applications. *Energy Proc* 2014;49:1420–8.
- [11] Peterseim JH, White S, Tadros A, Hellwig U. Concentrated solar power hybrid plants, which technologies are best suited for hybridisation? *Renew Energy* 2013;57:520–32.
- [12] Dersch J, Geyer M, Herrmann U, Jones SA, Kelly B, Kistner R, et al. Trough integration into power plants – a study on the performance and economy of integrated solar combined cycle systems. *Energy* 2004;29:947–59.
- [13] Bakos GC, Parsa D. Technoeconomic assessment of an integrated solar combined cycle power plant in Greece using line-focus parabolic trough collectors. *Renew Energy* 2013;60: 598–03.
- [14] Nezammahalleh H, Farhadi F, Tanhaemami M. Conceptual design and technoeconomic assessment of integrated solar combined cycle system with DSG technology. *Sol Energy* 2010;84:1696–705.
- [15] Antonanzas J, Jimenez E, Blanco J, Antonanzas-Torres F. Potential solar thermal integration in Spanish combined cycle gas turbines. *Renew Sust Energy Rev* 2014;37:36–46.
- [16] Antonanzas J, Alia-Martinez M, Martinez-de-Pison FJ, Antonanzas-Torres F. Towards the hybridization of gas-fired power plants: a case study of Algeria. *Renew Sust Energy Rev* 2015;51:116–24.
- [17] Trad A, Ali M Ameziane Ait. Determination of the optimum design through different funding scenarios for future parabolic trough solar power plant in Algeria. *Energy Convers Manage* 2015;91:267–79.
- [18] Yan Q, Hu E, Yang Y, Zhai R. Evaluation of solar aided thermal power generation with various power plants. *Int J Energy Res* 2011;35:909–22.
- [19] Peng S, Wang Z, Hong H, Xu D, Jin H. Exergy evaluation of a typical 330 MW solar-hybrid coal-fired power plant in China. *Energy Convers Manage* 2014;85:848–55.
- [20] Turchi CS, Ma Z. Co-located gas turbine/solar thermal hybrid designs for power production. *Renew Energy* 2014;64:172–9.
- [21] Guédez R, Spelling J, Laumert B. Enhancing the economic competitiveness of concentrating solar power plants through an innovative integrated solar-combined cycle with thermal energy storage. *J Eng Gas Turb Power* 2015;137:041701.
- [22] Spelling J, Laumert B, Fransson T. Advanced hybrid solar tower combined-cycle power plants. *Energy Proc* 2014;49:1207–17.
- [23] Quero M, Korzynietz R, Ebert M, Jiménez AA, del Río A, Brioso JA. Solugas – operation experience of the first solar hybrid gas turbine system at MW scale. *Energy Proc* 2014;49:1820–30.
- [24] Zhu G, Neises T, Turchi C, Bedilion R. Thermodynamic evaluation of solar integration into a natural gas combined cycle power plant. *Renew Energy* 2015;74:815–24.
- [25] Gülen SC. Second law analysis of integrated solar combined cycle power plants. *J Eng Gas Turb Power* 2015;137: 051701-1-9.
- [26] Ojo CO, Pont D, Conte E, Carroni R. Performance evaluation of an integrated solar combined cycle. In: *Proceedings of ASME Turbo Expo 2012*; 2012 June 11–15, Copenhagen, Denmark.
- [27] Pihl E, Spelling J, Johnsson F. Thermo-economic optimization of hybridization options for solar retrofitting of combined-cycle power plants. *J Sol Energy* 2014;136: 021001-1-9.
- [28] Thermoflex/Peace software release 24. Thermal Engineering Software for the Power Industry. Thermoflow Inc. 2 Willow Street, Suite 100, Southborough, MA 01745–1020, USA.
- [29] Manente G, Rech S, Lazzaretto A. On the optimum integration of solar energy into natural gas combined cycles. In: *Proceedings of ECOS2015: the 28th international conference on efficiency, cost, optimization, simulation and environmental impact of energy systems*; 2015 June 30–July 3, Pau, France.
- [30] Alus M, Petrovic MV. Optimization of parameters for heat recovery steam generator (HRSG) in combined cycle power plants. Technical presentation at Powerplants 2010: conference on power plants; 2010 October 26–29, Vrnjicka Banja, Serbia.
- [31] Pauschert D. Study of Equipment Prices in the Power Sector. Energy Sector Management Assistance Program, ESMAP Technical Paper 122/09, The International Bank for Reconstruction and Development, Washington, December; 2009.
- [32] Turton R, Bailie RC, Whiting WB, Shaiwitz JA. *Analysis, synthesis, and design of chemical processes*. 3rd ed. Boston: Prentice Hall; 2009.